Corrosion-Fatigue Behavior of Aluminum Alloy 5083-H131 Sensitized at 448 K (175 °C)

RONALD L. HOLTZ, PETER S. PAO, ROBERT A. BAYLES, THOMAS M. LONGAZEL, and RAMASIS GOSWAMI

The fatigue crack growth behavior of aluminum alloy 5083-H131 has been systematically studied as a function of degree of sensitization for aging at 448 K (175 °C). Fatigue crack growth rates were measured at load ratios of 0.1 and 0.85, in vacuum, air, and a corrosive aqueous environment containing 1 pct NaCl with dilute inhibitor. Sensitization does not affect the fatigue crack growth behavior of Al 5083-H131 significantly in vacuum or air, at low- or high-load ratio. For high-load ratio, in the 1 pct NaCl + inhibitor solution, the threshold drops by nearly 50 pct during the first 200 hours of aging, then it degrades more slowly for longer aging times up to 2000 hours. The change in aging behavior at approximately 200 hours seems to be correlated with the transition from partial coverage of the grain boundaries by β Al$_3$Mg$_2$ phase, to continuous full β coverage. ASTM G-67 mass loss levels below approximately 30 mg/cm^2 do not exhibit degraded corrosion-fatigue properties for $R = 0.85$, but degradation of the threshold is rapid for higher mass loss levels.

I. INTRODUCTION

ALUMINUM alloy 5083 is a commercial Al-4.5 pct Mg-1 pct Mn wrought alloy that derives its strength from magnesium solute hardening and strain hardening.[1] The 5083 and other 5xxx alloys are used in ship structures[2,3] because they have high specific strength, are weldable, and have good general corrosion resistance in marine environments.[4] However, these alloys can become *sensitized* to intergranular corrosion (IGC) and stress-corrosion cracking (SCC) when exposed to increased temperature [above 323 K (50 °C)] for prolonged periods of time.[5–8] This has obvious disadvantages for marine applications.[9] The IGC/SCC is known to be associated with the formation of β phase (Al$_3$Mg$_2$) on the grain boundaries.[5] The presence of β phase is detrimental to the alloy's IGC resistance because β is anodic with respect to aluminum,[10] and it is thought that high rate selective dissolution of the β occurs in chloride solutions.[6,7] A good review of the factors involved and mechanisms influencing IGC/SCC in Al-Mg alloys is provided by Jones.[11]

Although the precipitation of β from solid-solution Al-Mg alloys[5–7,12–17] and the damaging effect of grain boundary β precipitation and sensitization on IGC/SCC in 5xxx-series aluminum alloys[5–8,18–26] are well known,

little systematic information exists on the effect of grain boundary β on the fatigue crack growth of sensitized Al 5083 under cyclic fatigue loading conditions for both high and low load ratio, in various environments. A recent paper by Brosi and Lewandowski[27] tabulates the thresholds of Al 5456 measured in air only, for several load ratios, showing only minor changes of the fatigue thresholds with different degrees of sensitization, although more significant effects were noted on the Paris law exponents; however, L-T orientation was used, which is not the configuration most susceptible to intergranular corrosion.[8] Menzemer and Srivatsan[28] studied the effects of air, water vapor, and oxygen on as-received 5456-H116, also on L-T orientation, at $R = 0.1$, but sensitized material was not included in the study. Van Kranenburg et al.[29] measured the fatigue thresholds of as-received Al 5083 in air and seawater but also did not measure sensitized material. An older work by Ford[30] reported the results of an Al-7 pct Mg alloy aged at 423 K (150 °C) for 4 hours (thus probably sensitized) in both air and aqueous environments, but only one load ratio $R = 0$ is reported. Donald[31] more recently reported a wide-ranging study of fatigue crack growth results for 5083-H321 and 5083-H116 marine service alloys, in air and seawater, for a range of frequencies from 0.05 to 24 Hz; however, the transverse-longitudinal (TL) orientation was used, only one load ratio of 0.1 was investigated, and the data were not all taken down to the threshold regime. The sensitized alloy was not measured.

Thus, the objective of this study was to determine comprehensively the fatigue crack growth behavior of Al 5083 in several environments, at both high and low load ratio, and for sensitization conditions. Fatigue crack growth rates were measured for both as-received and highly sensitized condition at low load ratio

RONALD L. HOLTZ, Senior Physicist and PETER S. PAO, Senior Metallurgist, are with the Multifunctional Materials Branch, Naval Research Laboratory, Washington, DC 20375. Contact e-mail: ronald.holtz@nrl.navy.mil ROBERT A. BAYLES, Senior Metallurgist and THOMAS M. LONGAZEL, Materials Engineer, are with the Center for Corrosion Science and Engineering, Naval Research Laboratory. RAMASIS GOSWAMI, Senior Scientist, is with SAIC, Incorporated, Washington, DC 20375.
Manuscript submitted March 31, 2011.
Article published online August 30, 2011.

($R = 0.1$) and high load ratio ($R = 0.85$) to determine the basic behaviors when the loading is dominated by high cyclic amplitude, ΔK, vs high peak load, K_{MAX}, with small cyclic amplitude. The effects of environment were evaluated by measuring in high vacuum, air and an aqueous solution containing NaCl, and an inhibitor. High-vacuum measurements were included to represent an environment-free, intrinsic behavior for comparison. The initial findings for unsensitized and fully sensitized material were followed up by a systematic study of the corrosion-fatigue (CF) threshold at high R, in aqueous NaCl with inhibitor, as a function of aging time producing varying degrees of sensitization.[32]

The material used in this study was 58.4-mm thick AA5083-H131 plate, an armor-grade, wrought and strain-hardened material[33] provided by Alcoa (Alcoa Center, PA). The use of thick plate allowed for conventional fatigue testing with compact tension specimens loaded in the short-transverse (ST) direction, which is known to be the most susceptible to IGC and SCC problems.[8] The specimens were sensitized at 448 K (175 °C) for between 1 and 2000 hours. Transmission electron microscopy (TEM) was used to determine morphology and the continuity of grain boundary β phase of selected specimens. The relatively high temperature of 448 K (175 °C) was selected for the aging so that the full range of sensitized behavior could be explored efficiently. It has been shown elsewhere[34] that the corrosion-fatigue behavior correlates with the degree of sensitization, regardless of what aging temperatures are used. Lower aging temperatures merely require long aging times to achieve the same levels of sensitization.

II. MICROSTRUCTURE EVOLUTION WITH AGING

As noted in the introduction, there have been several studies of β precipitation in supersaturated Al-Mg alloys, so the basic phenomenology is well known. An overview of the precipitation behavior most germane to the current work is summarized by Searles et al.,[6] who analyzed comprehensively a 5083 alloy (temper not specified) aged at 423 K (150 °C) up to 333 hours. They reported the initial discrete precipitation of β particles and the formation of a continuous grain boundary β phase by 189 hours, but at 262 hours and longer, the grain boundary phase was broken up and discontinuous. The details of β phase evolution in the specific 5083 alloy and H131 initial temper, which was the subject of this study, have been reported previously[35,36] and generally are consistent with Searles et al.[6] Herein, we review briefly those previously published results to provide the microstructural context for the discussion of the corrosion-fatigue behaviors.

Figure 1(a) shows a typical grain boundary of the as-received Al 5083-H131. Note, in particular, that there is no β phase at the grain boundary in the as-received Al 5083-H131. After aging at 448 K (175 °C), the β phase starts to form on the grain boundaries. After 1 hour aging at 448 K (175 °C), discrete β precipitates start to form along the grain boundaries, as shown in Figure 1(b).
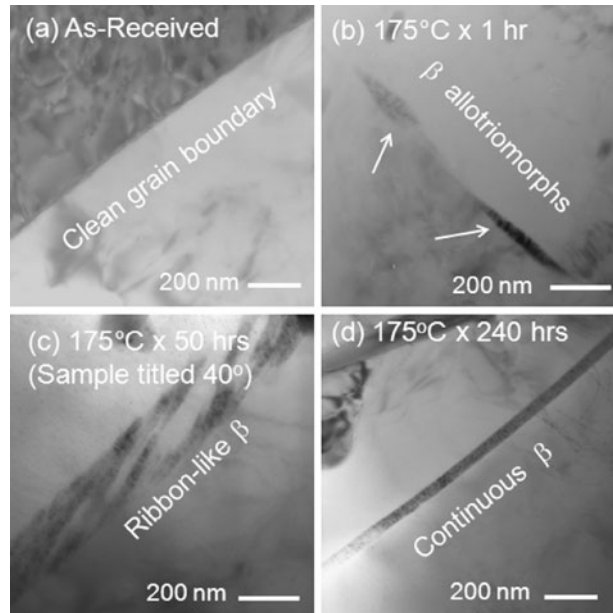

Fig. 1—Basic stages of the microstructure evolution of β-Al$_3$Mg$_2$ in Al 5083-H131 aged at 448 K (175 °C). The condition depicted in (d) is considered to be fully sensitized.

These fine-grain-boundary β precipitates are several hundred nanometers in length and up to approximately 60 nanometers in width. After aging at 448 K (175 °C) for 50 hours, the grain boundary β precipitate structure becomes more complex, forming a ribbon-like morphology, as shown in Figure 1(c). In this figure, the sample has been tilted approximately 40 deg so that it is an oblique view of the β phase on the grain boundary through the thickness of the TEM sample. As shown in Figure 1(c), the grain boundary is not fully covered by the β phase at this stage, but it is possible that the precipitates are continuous over length scales larger than the TEM sample thickness. Similar complex grain boundary β microstructures have been reported recently by Davenport et al.[17] for a 5182 alloy aged at 423 K (150 °C) for 50 hours. Only after a long period of aging greater than approximately 200 hours do β precipitates coalesce and the grain boundaries generally become fully covered with β phase with a thickness around 100 to 200 nm. An example of such a continuous grain boundary β phase after 240 hours aging at 448 K (175 °C) is shown in Figure 1(d).

The examination of multiple specimens aged for various periods of times indicates that generally the grain boundary β phase becomes continuous and fully covered after approximately 200 hours aging at 448 K (175 °C), and generally it is discontinuous and/or partially covered for shorter aging times. At longer aging times over 200 hours, the β phase continues to thicken, but at a lower rate.

III. FATIGUE CRACK GROWTH EXPERIMENTAL DETAILS

For fatigue crack growth studies, 12.7-mm-thick, S-L oriented, 58.4-mm-wide wedge-opening-load fracture

mechanics specimens were used. With the S-L orientation, the crack propagation direction is parallel to the rolling direction, loading is in the short-transverse direction, and the crack plane is in the midplane of the thick plate. This configuration was selected because loading in the ST direction is known to be the most susceptible to stress corrosion cracking.[8] ASTM E-647[37] fatigue tests were conducted with cyclic load frequency of 10 Hz, using a sine waveform and a stress ratio R of either 0.1 or 0.85. The fatigue crack length was monitored continuously by a compliance technique. Thresholds are determined by the ASTM E-647 method, *i.e.*, defined as stress intensity amplitude at a crack growth rate of 1×10^{-10} m/cycle.

The tests in high vacuum were done in a turbomolecular pumped vacuum chamber at a base pressure typically at 6.7×10^{-6} Pa. A residual gas analysis showed that the major constituents are approximately half nitrogen and half water vapor, with oxygen or other species being present in trace amounts. The tests in air were conducted in laboratory air at ambient laboratory temperature around 295 K (22 °C) and 42 pct relative humidity.

The corrosive environment fatigue crack growth experiments were conducted by an immersion of the specimens during testing in 1 pct NaCl solution with a chromate inhibitor (0.02 M $Na_2Cr_2O_7$, 0.07 M $NaC_2H_3O_2$, and $HC_2H_3O_2$ with pH = 4).[20,38] To avoid possible confusion about the composition of the solution used for our testing, we refer to this mixture as 1 pct NaCl/Inh in this article.

It was noticed during the initial several fatigue tests of the sensitized 5083 samples in pure 1 pct NaCl solution, without inhibitor, that there was a buildup of gel-like corrosion products (the hydroxide products of the dissolution of β in saltwater[39]) on the surface of the specimens as well as within the cracks. The viscous corrosion products can affect the environment at the crack tip, for example, by impeding the solute transport through the crack preventing fresh solution from penetrating to the crack tip[40,41] or affecting the local stress intensity through hydrostatic pressure effects.[42]

To avoid such problems and thus obtain results more representative of intrinsic material behavior, the dilute chromate inhibitor solution was used. The particular inhibitor selected is a solution that has been used by Alcoa[20,38] for continuous immersion stress-corrosion cracking tests. Jones *et al.*[22] also described the use of a potassium chromate solution for SCC testing of Al-Mg alloys. The chromate solution acts to passivate the exposed crack surfaces. When a passivated crack is loaded in tension, the passivated layer is broken at the crack tip, and at sufficiently high frequency, it does not reform quickly enough for stable passivation.[43,44] (We should note that TEM studies by Jones *et al.*[45] suggest a somewhat more complicated effect on the β phase in Al-Mg alloys exposed to inhibitor, involving conversion of the Al_3Mg_2 to Al_2O_3.) Thus, the underlying alloy at the crack tip is exposed to the NaCl after loading, so that the environmental interaction can occur, whereas the crack faces in the wake remain passivated to reduce corrosion product buildup.

Several experiments were conducted to compare results with and without inhibitor. Figure 2 shows several tests on as-received and sensitized [448 K (175 °C) for 240 hours, degree of sensitization [DOS] approximately 40 mg/cm^2] samples, with and without inhibitor. The as-received, or unsensitized, material is indicated by "A" and corresponds to the type of microstructure shown in Figure 1(a). The sensitized material is denoted by "S" and is obtained with an aging of 240 hours at 448 K (175 °C), and it corresponds to the microstructure shown in Figure 1(d). It is observed that the crack growth rate of unsensitized material is not affected, regardless of the presence of the inhibitor. In the case of the sensitized material, without inhibitor there would seem to be little or no change of the near-threshold behavior. With inhibitor, crack growth rates at low-stress intensity amplitude increase, and the threshold decreases significantly. This behavior would otherwise seem to be counterintuitive if the corrosion product plugging the crack were not taken into account. At high amplitude, where the crack geometry is less
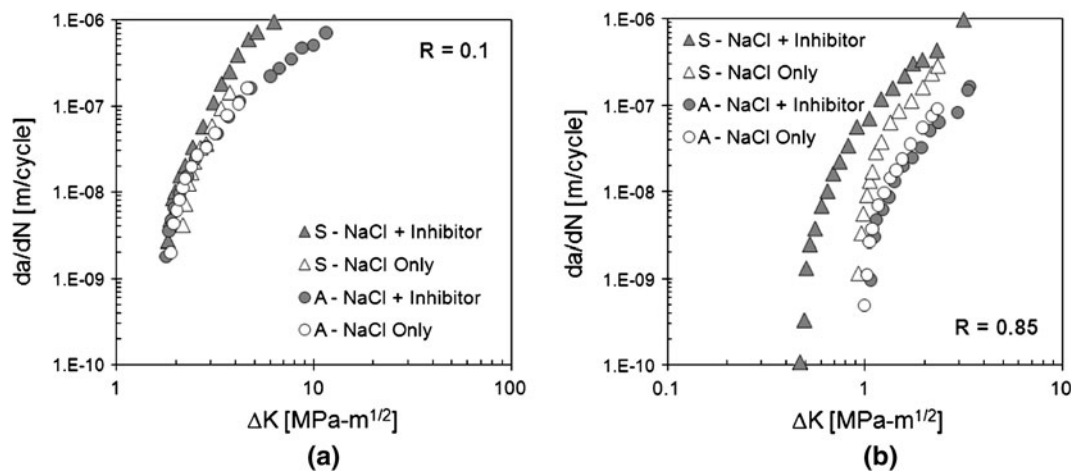

Fig. 2—Effect of the chromate inhibitor solution, with 1 pct NaCl, on the corrosion-fatigue behavior of as-received and highly sensitized samples. "A" refers to as-received or unsensitized condition, and "S" refers to highly sensitized condition [448 K (175 °C) for 240 h]. (*a*) *R* = 0.1 and (*b*) *R* = 0.85.

stagnant and corrosion product blocking of the crack should be less significant, the da/dn without inhibitor approaches that with inhibitor.

An NaCl concentration of 1 pct was used for these experiments. It was verified experimentally on unsensitized samples and samples sensitized at 448 K (175 °C), that there is no significant difference between the thresholds for 1 pct NaCl/Inh and 5 pct NaCl/Inh, as indicated in Figure 3. The NaCl concentrations less than 0.1 pct have diminishing effect on the fatigue behavior. Based on these data, it is clear that the 1 pct NaCl/Inh solution would give the same result as, for example, 3.5 pct NaCl, within experimental uncertainties.[34]

Furthermore, that the changes in threshold for sensitized material are caused by the NaCl and not the inhibitor is confirmed by Figure 3. As the NaCl concentration decreases, with the same inhibitor solution, the threshold approaches the same value as unsensitized material.

IV. FATIGUE CRACK GROWTH RESULTS

Figure 4(a) shows the fatigue crack growth behavior at $R = 0.1$ in vacuum, air, and 1 pct NaCl/Inh. The as-received, or unsensitized, material is indicated by "A" and corresponds to the type of microstructure shown in Figure 1(a). The sensitized material is denoted by "S" and is obtained with an aging of 240 hours at 448 K (175 °C), and it corresponds to the microstructure shown in Figure 1(d). Several behaviors are notable. The thresholds of both sensitized and unsensitized material, in both air and 1 pct NaCl/Inh, are all the same. Thus, empirically, at low R, sensitization does not play a role in the fatigue crack growth thresholds. The air and NaCl/Inh thresholds are lower than the thresholds for vacuum, indicating that there is an environment effect acting in both air and NaCl/Inh, presuming that the vacuum data represent inert environment behavior. It is interesting that the aqueous environment threshold is the same as in air, and this will be discussed further, below. Away from the thresholds, crack growth rates are always higher in the 1 pct NaCl/Inh than in air, and da/dn in air is higher than in vacuum. In NaCl/Inh at intermediate ΔK, sensitization always increases the crack growth rate. At high ΔK, where K_{MAX} is approaching the fracture toughness of the material, the curves all merge. At $R = 0.85$, shown in Figure 4(b), the trends of crack growth rates for vacuum and air are similar to the trends at R = 0.1. In particular, sensitization does not have a significant effect in either air or vacuum, but the air thresholds are much lower than in vacuum indicating a significant environment effect even in air. In 1 pct NaCl/Inh, however, there is a large difference between unsensitized and sensitized material. As at $R = 0.1$, unsensitized material in NaCl/Inh has the same threshold as in air, and the crack growth rates for intermediate ΔK are always higher in NaCl/Inh than in air, whereas the sensitized material in NaCl/Inh shows a large increase in the crack growth rates.
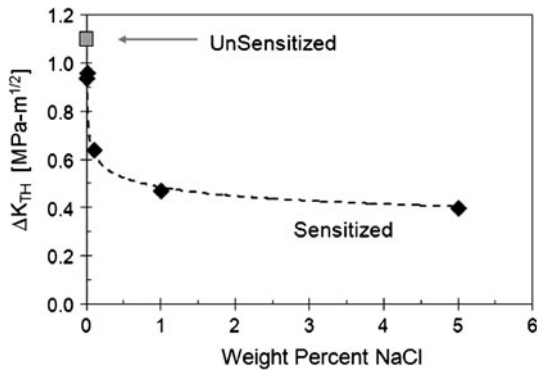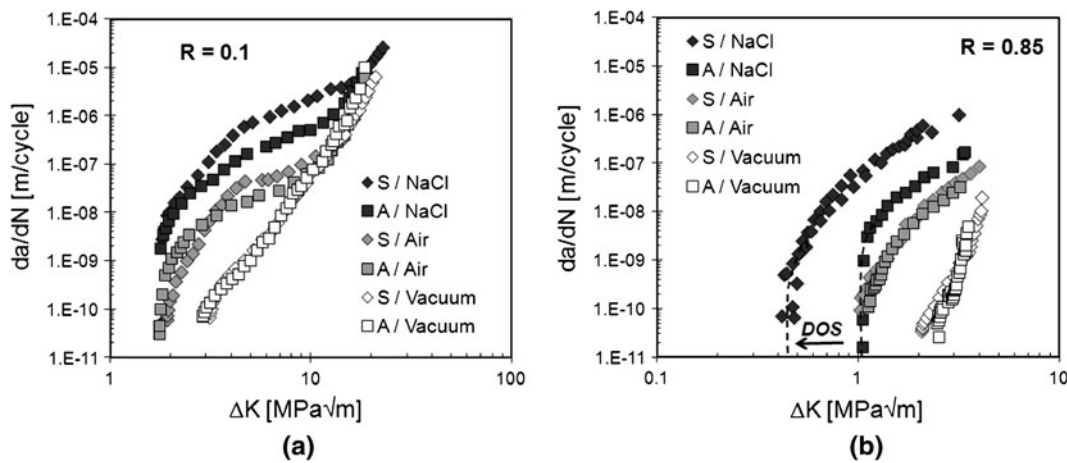

Fig. 3—Effect of NaCl concentration, with the inhibitor solution described in the text, on the corrosion-fatigue thresholds of highly sensitized samples at $R = 0.85$.

Fig. 4—Fatigue crack growth rates at $R = 0.1$ (*a*) and $R = 0.85$ (*b*) in vacuum, air, and 1 pct NaCl + inhibitor. In the legend, "A" refers to as-received or unsensitized condition, and "S" refers to fully sensitized condition. The DOS and the arrow indicate the shift of threshold with increasing sensitization.

As indicated by the figure, the threshold in NaCl/Inh decreases by a factor of two from unsensitized to sensitized condition.

To investigate how the threshold depends on aging time and degree of sensitization, we prepared a series of specimens aged at 448 K (175 °C) for various times ranging from 1 hour to 2000 hours. The results are shown in Figure 5. ΔK_{TH} decreases rapidly for the first 200 hours of aging then continues to decrease at a slower rate for additional aging. The slope changes at approximately the aging time corresponding to the 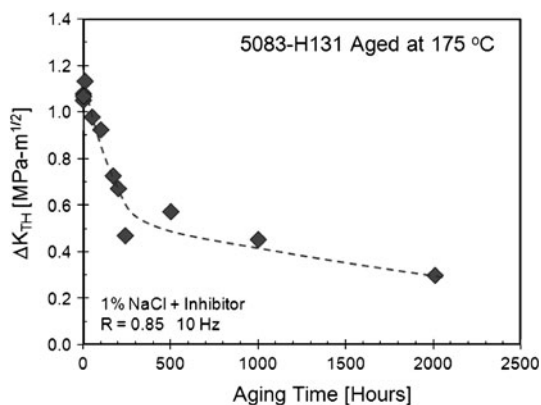change from partial/discontinuous β coverage of the grain boundaries to full/continuous coverage. TEM observations of the longer aged samples have shown that once the grain boundary coverage is complete, the β phase thickens slowly with additional aging.

Additionally, we measured the SCC thresholds, K_{1SCC}, in the same 1 pct NaCl/Inh solution, of the as-received and fully sensitized material. The tests were rising stress step loading tests (ASTM E1681-03[46]). The K_{1SCC} values were determined to be approximately 20 and 3 MPa√m, for the as-received and sensitized (240 hours at 448 K [175 °C]) materials, respectively. These values are the same as characterization provided to us by Alcoa along with the sample material, for S-L oriented, double-cantilever beam specimens under constant displacement, with drop-wise exposure to 3.5 pct NaCl.[47]

Fig. 5—Fatigue crack growth thresholds at $R = 0.85$ in 1 pct NaCl + inhibitor *vs* aging time at 448 K (175 °C).

V. FRACTOGRAPHY

A fractographic examination of the crack faces was performed by scanning electron microscopy (SEM). Here, we include crack face images near the threshold regime, which is the region of interest for analyzing the fatigue threshold results. In vacuum, the cracking is transgranular for both sensitized and unsensitized material, and for both $R = 0.1$ and 0.85, as shown in Figure 6. Furthermore, the cracking mode is the same for all ΔK. In air (Figure 7), the fractography typically shows mixed transgranular with intergranular cracking
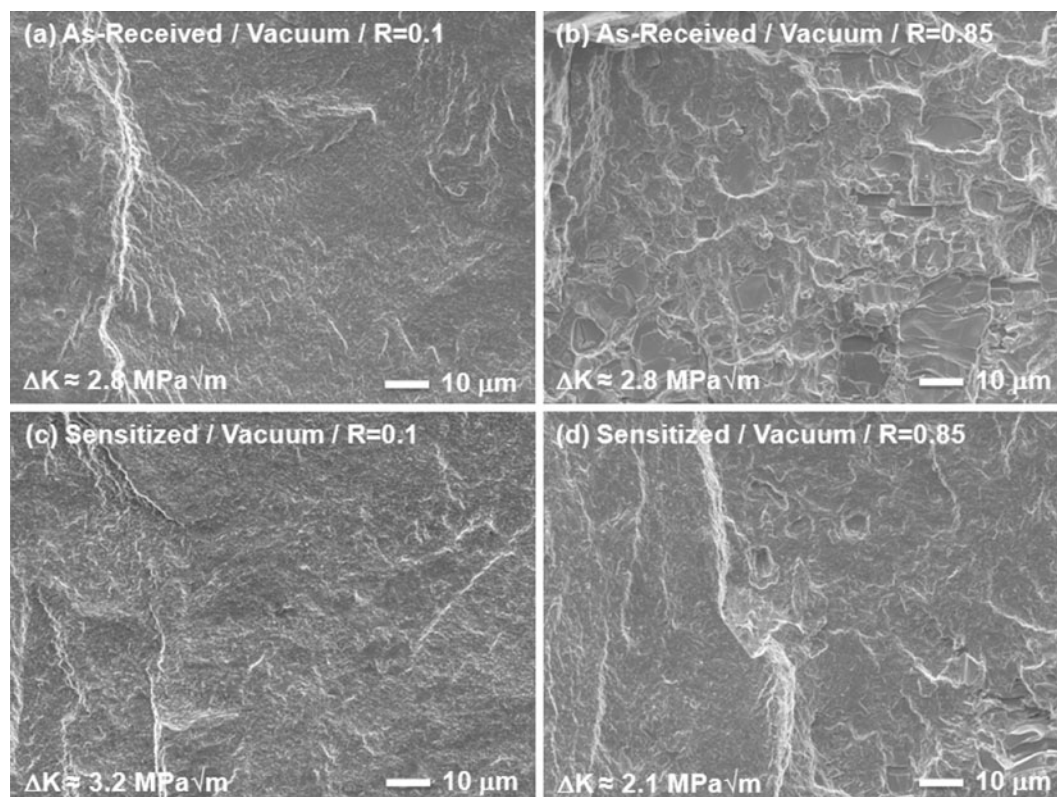

Fig. 6—SEM fractographs in the near-threshold regime for samples tested in high vacuum. (*a*) As received at $R = 0.1$, (*b*) as received at $R = 0.85$, (*c*) sensitized at $R = 0.1$, and (*d*) sensitized at $R = 0.85$.
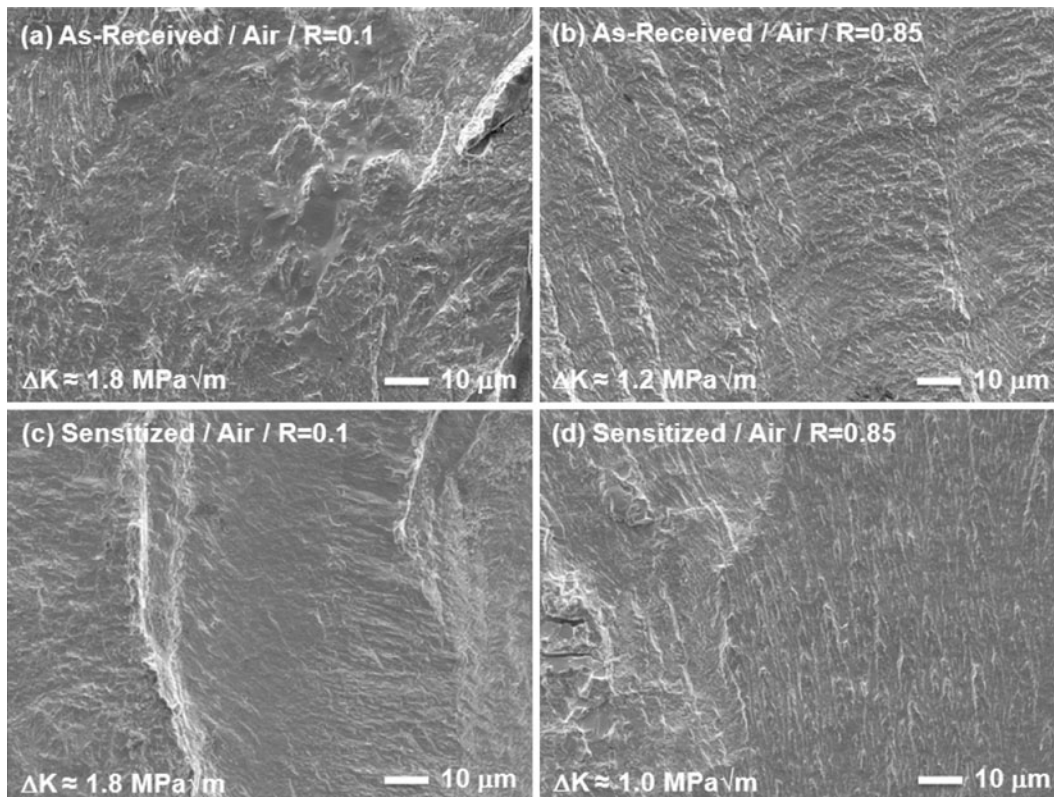
Fig. 7—SEM fractographs in the near-threshold regime for samples tested in air. (*a*) As received at $R = 0.1$, (*b*) as received at $R = 0.85$, (*c*) sensitized at $R = 0.1$, and (*d*) sensitized at $R = 0.85$.

at $R = 0.1$ but purely transgranular at $R = 0.85$. At high ΔK (not shown), the fracture mode trends are the opposite, mostly transgranular at low R and mixed intergranular and transgranular at high R. The fracture modes in all cases are the same for both sensitized and unsensitized specimens. In the aqueous 1 pct NaCl/Inh environment, near threshold as well as higher ΔK, the fracture surfaces are always intergranular, for both sensitized and unsensitized, at both high and low R, as shown in Figure 8. At high ΔK (not shown), the fracture mode at $R = 0.1$ becomes transgranular but remains intergranular at $R = 0.85$.

The fractography indicates that the cracking *mode* is not sensitive to the presence of grain boundary β in any of the environments, regardless of load ratio or stress intensity amplitude. This is consistent generally with the observations that the near-threshold fatigue crack growth rates generally do not depend much on sensitization, either, with the exception of high R in the aqueous corrosive environment. If the vacuum behavior can be taken as an indication of environment-free behavior, then the intrinsic behavior is transgranular cracking. In air, where there should be somewhat of an environment effect from water vapor, some intergranular attack occurs presumably in competition with the transgranular cracking associated with intrinsic behavior. In the aqueous environment, the anodic dissolution of the β phase in the sensitized material contributes to the crack tip behavior and the cracking becomes entirely intergranular at low crack growth rates, but at low R and high crack growth rates, the β is not dissolved entirely.

The SEM micrographs do not show the presence of β phase unambiguously. There is not much contrast between aluminum and Al_3Mg_2 in the SEM, there is still Mg present in the aluminum grains, and the grain boundary coverage is thin, at most 200 nm for highly sensitized samples. In the cases of transgranular cracking in vacuum and air, the β phase coverage on the grains is not visible because it is not exposed by the crack path. In the case of tests performed in the 1 pct NaCl/Inh solution, where the cracking is intergranular, the β phase either has been dissolved away or converted to an oxide by the action of the inhibitor, and thus it would not be recognizable as β on the surface of the crack face. For sensitized samples tested in air, at low load ratio, in regions where intergranular cracking occurred, there may be some surface irregularities possibly associated with the β phase coverage. However, more specialized experiments will be needed to confirm whether residual β is present on the crack faces.

VI. DISCUSSION

The observation that the fatigue threshold in NaCl/Inh is not affected by sensitization at low R but is strongly affected at high R can be understood phenomenologically by referring to Figure 9. As mentioned in the introduction, it is well known that the 5xxx series of Al-Mg alloys in the sensitized condition are susceptible to SCC at a high enough stress intensity, $K > K_{1SCC}$. When K is less than K_{1SCC}, only cyclic fatigue processes
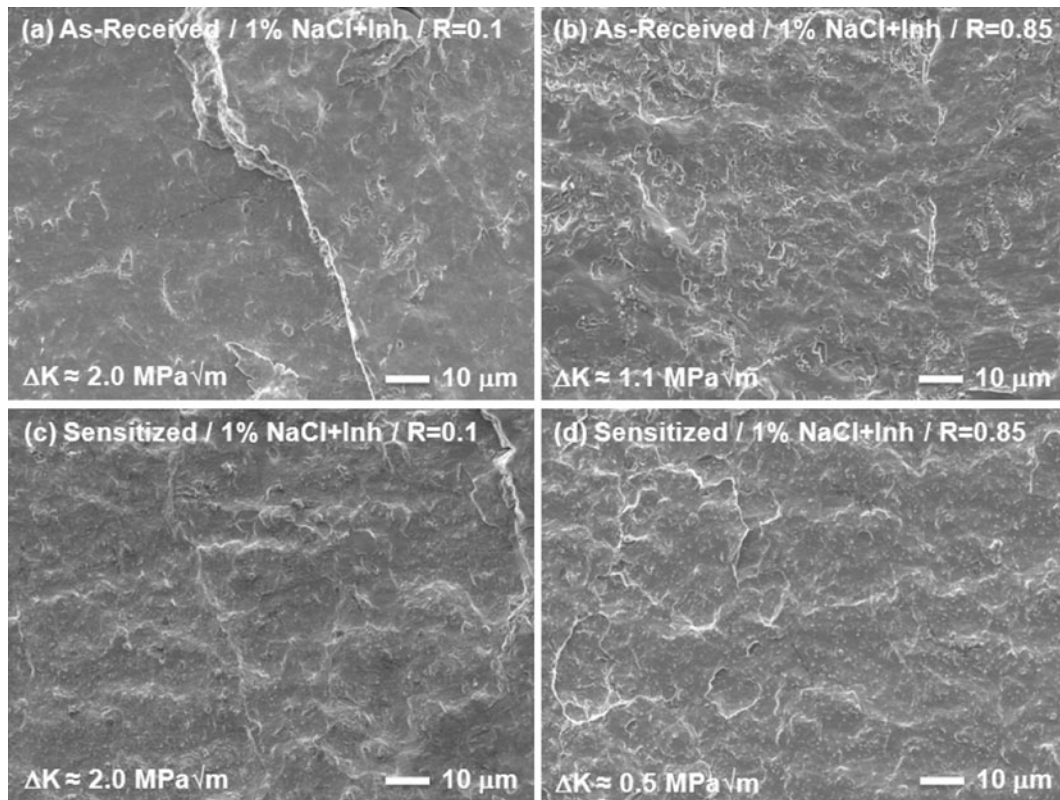
Fig. 8—SEM fractographs in the near-threshold regime for samples tested in 1 pct NaCl plus inhibitor. (*a*) As received at $R = 0.1$, (*b*) as received at $R = 0.85$, (*c*) sensitized at $R = 0.1$, and (*d*) sensitized at $R = 0.85$.
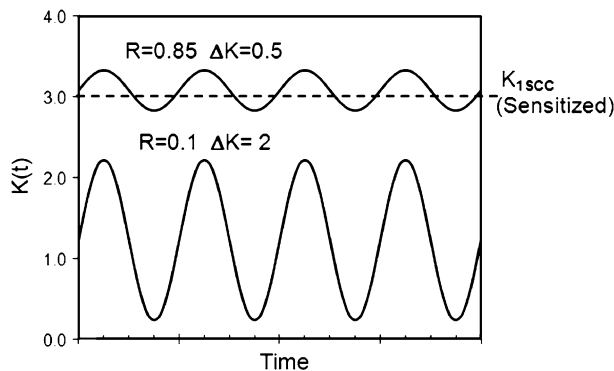

Fig. 9—Schematic indicating why thresholds at $R = 0.1$ are not affected by sensitization, whereas the $R = 0.85$ thresholds are strongly affected. For $R = 0.1$ at the low ΔK values near threshold, the load cycle is below the SCC threshold K_{1SCC}. At high R, however, some portion of the cycle is above K_{1SCC} thus is affected strongly.

are growing the crack, and we presume that a threshold is associated with that cyclic-only process, ΔK_{CFTH}. The fatigue-only case would correspond to the unsensitized material in NaCl/Inh, where $\Delta K_{CFTH} \approx 1.8$ at $R = 0.1$ and $\Delta K_{CFTH} \approx 1.0$ at $R = 0.85$. We presume that this cyclic mechanism is driven by the same hydrogen-embrittlement cracking mechanism that has been discussed for the Al 5456 alloy.[28] The K_{1SCC} in the fully sensitized condition of the Al 5083-H131 is approximately 3 MPa√m. At $R = 0.1$, with $\Delta K \approx 2$ MPa√m, near the observed thresholds, the entire load cycle is

lower than K_{1SCC}, and therefore the behavior is dominated by cyclic processes only, such that the crack stops growing when ΔK falls below ΔK_{CFTH}. At higher ΔK and $R = 0.1$, SCC contributes to the crack growth rate whenever K_{MAX} exceeds K_{1SCC}, and the crack growth rates of sensitized material thus will be higher than unsensitized material. In contrast, at $R = 0.85$, some portion of the load cycle, or even all of the load cycle, is above K_{1SCC}, and thus, SCC contributes to the crack growth during those portions of the loading cycle.

Thus, a full analysis of the corrosion-fatigue behavior of the sensitized 5083 alloy requires consideration of the superimposed effects of corrosion-fatigue and stress-corrosion cracking.[48] Various models for the effects of environment on corrosion fatigue were reviewed elsewhere.[49,50] What is apparent from this body of literature is that, generally, the combined actions of CF and SCC for finite crack growth rates are a complex and difficult problem. Additionally, it is noted that none of these models include threshold behaviors explicitly, and thus, they do not help directly in the interpretation of the current data.

Gnyp and Pokhmursky[51] considered threshold behavior under the combined action of CF and SCC, and they argued that a "cyclic corrosion cracking" threshold ΔK_{ISCFC} is needed to describe the threshold behavior. In their model, the materials that are subject to static corrosion cracking as well as cyclic corrosion cracking require two characteristic, independent parameters, ΔK_{ISCFC}, as well as K_{1SCC}. It seems clear that the

corrosion-fatigue threshold measured in the current work would be considered to be an example of ΔK_{ISCFC}. The consequent interpretation is that ΔK_{ISCFC} is not an intrinsic property but rather the apparent threshold that results from the superposition of an intrinsic CF behavior with the SCC behavior, as we explain in more detail in the next section.

Any superposition model invoking combinations of terms representing additive contributions to the crack growth rates possesses the feature that the individual terms must all be greater than or equal to zero. The crack growth rates cannot be negative. The threshold behavior that is, defined as $da/dN = 0$ of such an additive superposition model, thus is simple, in principle, to analyze. The model of Wei and Simmons[52] explicitly has separate terms for CF and SCC contributions, which is needed for the present current, and it has been successful in accounting for frequency and water vapor pressure effects in some aluminum alloys. The Wei-Simmons model is essentially a summation of independent terms for inert materials behavior, a cyclic corrosion-fatigue behavior, and an intrinsic stress corrosion cracking behavior:

$$\left(\frac{da}{dN}\right)_{Total} = \left(\frac{da}{dN}\right)_{Inert} + \left(\frac{da}{dN}\right)_{CF} + \left(\frac{da}{dN}\right)_{SCC}$$

For the total crack growth rate to be zero in this case, that is, at threshold, all three terms must be separately zero.

In the current case, the "inert" term in the Wei-Simmons model does not contribute because the threshold in vacuum is much higher than in the 1 pct NaCl/Inh, leaving the separated terms for corrosion-fatigue, characterized by a cyclic-only fatigue threshold, which we term ΔK_{CFTH}, and stress corrosion cracking, which is characterized by a threshold for K_{MAX}, that is, K_{1SCC}. Physically, this means simply that a crack will not grow when two conditions are met simultaneously: The peak stress intensity is less than K_{1SCC} and the cyclic stress intensity is below ΔK_{CFTH}. In the current case, for $R = 0.85$, with $K_{1SCC} \approx 3$ MPa√m, the apparent ΔK_{TH} is $(1 - R)K_{1SCC} = 0.45$, which agrees with the measurements and is well below the cyclic-only threshold, $\Delta K_{CFTH} \approx 1$ MPa√m. Thus, the measured ΔK_{TH} values shown in Figure 6 are *apparent* thresholds resulting from the SCC contribution, which can be much less than the cyclic fatigue-only threshold ΔK_{CFTH}. In the unsensitized condition, however, the K_{1SCC} is too high to play a role at the threshold, except when K_{MAX} is over 20 MPa√m.

The variation of measured apparent threshold ΔK_{TH} with aging time can be understood phenomenologically via Figure 10. Figure 10 is a series of schematic representations of threshold behavior based on the superposition ideas outlined previously. The axes are approximately scaled to the observed threshold behavior. One way of representing fatigue threshold behavior is by plotting a "map" in ΔK vs K_{MAX} space (this is algebraically equivalent to the more customary practice of plotting ΔK vs R because $K_{MAX} = \Delta K/(1 - R)$).[52–54] For cyclic fatigue only, these plots are generally L-shaped curves, as indicated in Figure 10(a), such that
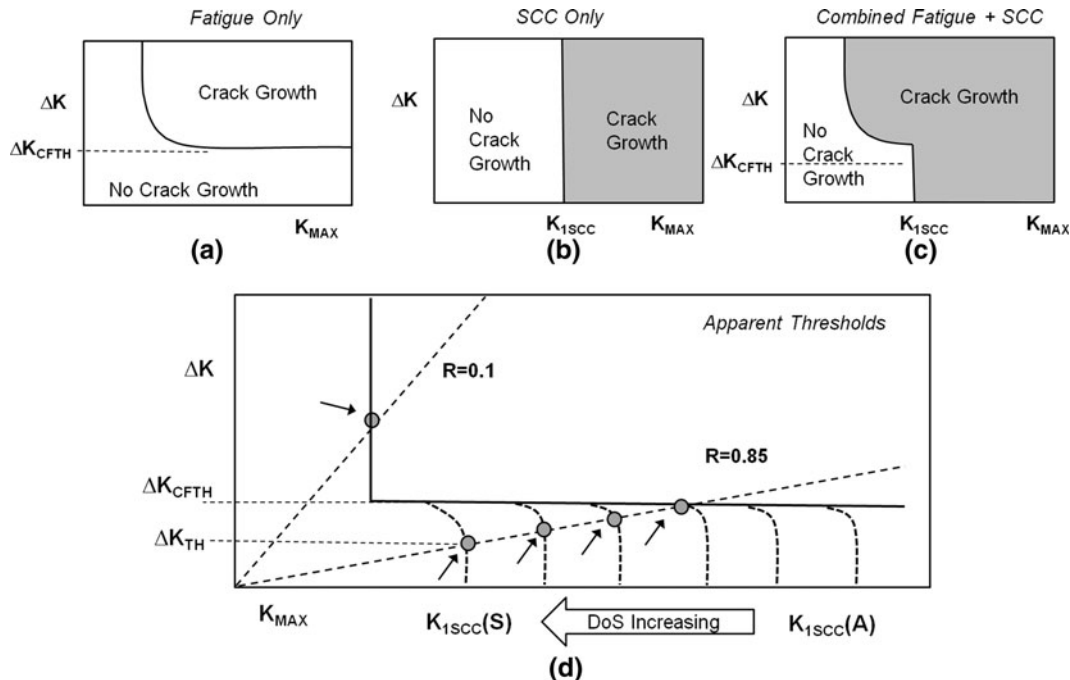

Fig. 10—Series of schematics suggesting a mechanism for why thresholds at $R = 0.1$ are not affected by changes in the stress corrosion cracking threshold, K_{1SCC}, whereas the $R = 0.85$ thresholds are affected strongly. (*a*) Schematic representation of typical fatigue threshold behavior, after the approach of Sadananda and Vasudevan.[53] (*b*) SCC behavior showing a threshold for K_{MAX} at K_{1SCC}. (*c*) Simple superposition of the fatigue and SCC behaviors. (*d*) As K_{1SCC} decreases with aging, the intersection of the threshold curves with the $R = 0.85$ line; that is, the apparent corrosion-fatigue threshold decreases progressively below ΔK_{CFTH}.

combinations of ΔK and K_{MAX} above and to the right of the curve produce crack growth, and combinations of ΔK and K_{MAX} below and left of the curve do not produce crack growth.[52,54] For our immediate purposes, which only concern the thresholds at $R = 0.1$ and $R = 0.85$, we do not need to know the exact shape of the curve at intermediate R. Figure 10(b) shows a threshold map for SCC only, where crack growth occurs for $K_{MAX} > K_{1SCC}$ and there is no crack growth for K_{MAX} below K_{1SCC}. If the SCC map is superimposed on the CF map and assuming no interactions, the combined threshold map of Figure 10(c) results. At low enough K_{MAX}, cyclic fatigue dominates, SCC plays no role, and the threshold follows the CF-only curve. At a high enough K_{MAX}, SCC dominates, and the threshold curve resembles the SCC only curve, in particular, intersecting $K_{MAX} = K_{1SCC}$ when $\Delta K = 0$. If interactions between CF and SCC are present, presumably the junction of the SCC and CF curves would be distorted somewhat to remove the sharp corner.[55–57] In other words, if K_{MAX} exceeds K_{1SCC}, the crack will grow regardless of what ΔK is; but if K_{MAX} is somewhat less than K_{1SCC}, the cyclic process dominates. For the intermediate levels of sensitization, between fully sensitized and unsensitized, we presume that the K_{1SCC} varies continuously with aging time. Figure 10(d) depicts a series of ΔK vs K_{MAX} maps suggesting what happens when K_{1SCC} drops with aging. The intersections of those curves with the line $R = 0.85$ gives the corresponding *apparent* corrosion-fatigue threshold produced by the superposition of a cyclic-only process with the K_{MAX}-only SCC process. This graphical representation described previously explains at least qualitatively the observed behavior of corrosion-fatigue thresholds with aging. The quantitative agreement also is pretty good for the highly sensitized material, where K_{1SCC} is about 3 MPa-$\sqrt{m}$. The diagram suggests that ΔK_{TH} should be approximately $1 - R = 15$ pct of K_{1SCC}, and in fact the measured thresholds for highly sensitized material are indeed approximately 0.45 MPa-$\sqrt{m}$. The implication is that at least at the threshold, any interaction or competition effects between CF and SCC are small in this alloy.

VII. RELATIONSHIP OF CORROSION FATIGUE THRESHOLD TO ASTM G67 MASS LOSS TEST

The customary method of characterizing the DOS of Al-Mg alloys is ASTM G-67,[58] which is commonly known as the nitric acid mass loss test (NAMLT). This test method involves immersing a sample in concentrated nitric acid for 24 hours and measuring the mass loss resulting from that immersion. The basis of the test is that the mass loss is associated with grains that fall out after the grain boundary β phase has been dissolved away by the acid. When the material is sensitized fully, the grain boundaries are covered fully with continuous layer of β; thus, the grains are more likely to fall out after the acid immersion. When the DOS is low and the β is not continuous or fully covering, the grains would be less likely to fall out. Thus, one would expect the

NAMLT to increase substantially when the grain boundary microstructure changes from discontinuous to continuous. In fact, as suggested in Figure 11, we find no evidence of a transition in NAMLT behavior corresponding to any transition in microstructure implied from TEM studies. This raises some questions about the rationale behind ASTM G67, although the test method is used widely and will remain a useful standard tool for characterization.

In Figure 12, the $R = 0.85$ corrosion-fatigue threshold is plotted *vs* the NAMLT values. For NAMLT of 30 mg/cm^2 and less, there is not much effect on the threshold. Above NAMLT of 30 mg/cm^2, the thresholds decrease rapidly. The transition from discontinuous/partial coverage to continuous/full coverage β on the grain boundaries occurs at approximately NAMLT of 40 mg/cm^2. This result suggests that, if one chooses to use ASTM G67 NAMLT values as an indicator of material condition, then a mass loss of approximately 30 mg/cm^2 should be considered the threshold above which the material properties are significantly degraded,
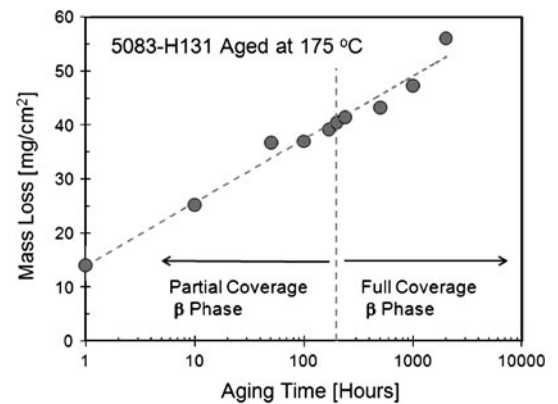

Fig. 11—ASTM G-67 nitric acid mass loss *vs* aging time for Al 5083-H131 aged at 448 K (175 °C). The approximate aging time corresponding to the observed transition between partial coverage/discontinuous β grain boundary phase and full coverage/continuous β phase is indicated (see text).
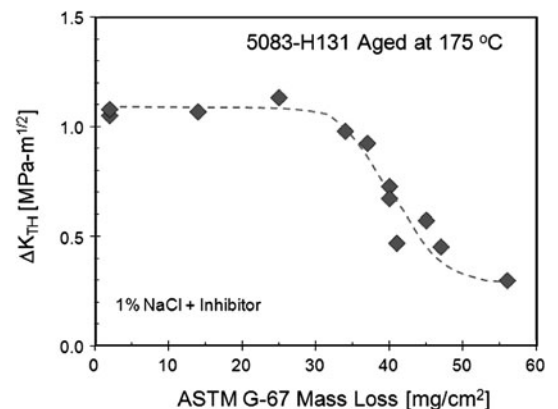

Fig. 12—The corrosion-fatigue threshold at $R = 0.85$ *vs* the ASTM G-67 nitric acid mass loss showing the degradation setting in for mass loss above 30 mg/cm^2.

at least for R approximately 0.85. The CF + SCC superposition arguments in the preceding section imply that this critical value of mass loss should depend on load ratio, *i.e.*, decreasing for higher load ratio and increasing for lower load ratio. Additional studies are underway to examine this prediction.

VIII. CONCLUSIONS

Sensitization does not affect the fatigue crack growth behavior of Al 5083-H131 significantly in vacuum or air, at low or high load ratio. In a corrosive environment of 1 pct NaCl plus chromate inhibitor, the threshold is not affected by sensitization at low R but is strongly affected at high R. There is a significant environmental enhancement of the crack growth rates in air, for both low and high R, relative to the behavior in vacuum.

For high R, in 1 pct NaCl/Inh, the apparent corrosion-fatigue threshold depends strongly on aging time at 448 K (175 °C). The threshold drops by nearly 50 pct during the first 200 hours of aging, and then degrades more slowly for longer aging times. The change in aging behavior at around 200 hours aging seems to be correlated with the transition from discontinuous or partial β phase coverage of the grain boundaries, to continuous and full β coverage.

These trends can be understood phenomenologically as the threshold behavior of a noninteracting, superposition of a corrosion-fatigue only process with a stress-corrosion cracking mechanism. This simple model accounts well for the observed trends as a function of sensitization of the corrosion-fatigue threshold at $R = 0.85$.

Based on our results, we suggest that an ASTM G-67 mass loss value in excess of approximately 30 mg/cm^2 would be indicative of substantially increased risk of corrosion-fatigue failure of this material for load ratios of approximately 0.8 to 0.9 in the presence of corrosive environment. ASTM G-67 mass loss levels below approximately 30 mg/cm^2 do not exhibit degraded corrosion-fatigue properties in our study. Although ASTM G-67 mass loss seems to provide for an indicator of corrosion-fatigue degradation, it may not correlate well with changes in the microstructure of grain boundary β.

REFERENCES

1. E.L. Huskins, B. Cao, and K.T. Ramesh: *Mater. Sci. Eng. A*, 2010, vol. 527, pp. 1292–98.
2. R.A. Sielski: *Ships and Offshore Structures*, 2008, vol. 3, pp. 57–65.
3. W.G. Babcock and E.J. Czyryca: *AMPTIAC Quart.*, 2003, vol. 7 (3), pp. 31–36.
4. G.C. Blaze: *Alcoa Green Letter: The 5000 Series Alloys Suitable for Welded Structural Applications*, Aluminum Corporation of America, New Kensington, PA, 1972.
5. E.H. Dix, W.A. Anderson, and M.B. Shumaker: *Corrosion*, 1959, vol. 15 (2), pp. 19–26.
6. J.L. Searles, P.I. Gouma, and R.G. Buchheit: *Metall. Mater. Trans. A*, 2001, vol. 32A, pp. 2859–67.
7. R.H. Jones, D.R. Bauer, M.J. Danielson, and J.S. Vetrano: *Metall. Mater. Trans. A*, 2001, vol. 32A, pp. 1699–1711.
8. F.S. Bovard: *Corrosion in Marine and Saltwater Environments II*, Eds. D.A. Shifler, T. Tsuru, P.M. Natishan, and S. Ito, vols. 2004–2014, Electrochemical Society, Pennington, NJ, 2005, pp. 232–243.
9. C.R. Wong, G.P. Mercier, and J.J. Deloach: *SeaFrame*, 2007, vol. 3 (2), pp. 18–20.
10. N. Birbilis and R.G. Buchheit: *J. Electrochem. Soc.*, 2005, vol. 152, pp. B140–51.
11. R.H. Jones: *J. Met.*, 2003, vol. 55 (2), pp. 42–46.
12. M. Fellerkniepmeier, K. Detert, and L. Thomas: *Z. Metallkunde*, 1964, vol. 55, pp. 83–87.
13. P.N.T. Unwin and R.B. Nicholson: *Acta Metall.*, 1969, vol. 17, pp. 1379–93.
14. L.I. Kaygorodova, B.N. Balandin, and N.N. Buynov: *Phys. Met. Metall.*, 1985, vol. 59, pp. 126–30.
15. T. Sato and A. Kamio: *Mater. Sci. Eng. A*, 1991, vol. A146, pp. 161–80.
16. H. Inagaki: *Z. Metallkunde*, 2005, vol. 96, pp. 45–53.
17. A.J. Davenport, Y. Yuan, R. Ambat, B.J. Connolly, M. Strangwood, A. Afseth, and G. Scamans: *Mater. Sci. Forum*, 2006, vols. 519–521, pp. 641–46.
18. M.F. Komarova, N.N. Buinov, and L.I. Kaganovi: *Phys. Met. Metall.*, 1973, vol. 36, pp. 358–64.
19. S. Osaki: *Technology Reports of the Yamaguchi University*, 1974, vol. 1 (3), pp. 347–48.
20. J.R. Pickens, J.R. Gordon, and J.A.S. Green: *Metall. Trans. A*, 1983, vol. 14A, pp. 925–30.
21. M. Popovic and E. Romhanji: *J. Mater. Process. Technol.*, 2002, vols. 125–126, pp. 275–80.
22. R.H. Jones, J.S. Vetrano, and C.F. Windisch: *Corrosion*, 2004, vol. 60, pp. 1144–54.
23. I.N.A. Oguocha, O.J. Adigun, and S. Yannacopoulos: *J. Mater. Sci.*, 2008, vol. 43, pp. 4208–14.
24. L. Tan and T.R. Allen: *Corros. Sci.*, 2010, vol. 52, pp. 548–54.
25. J. Gao and D.J. Quesnel: *Metall. Mater. Trans. A*, 2011, vol. 42A, pp. 356–64.
26. C.B. Crane and R. Gangloff: *DoD Corrosion Conf. Proc.*, NACE International, Houston, TX, Paper 20175, 2011, in press.
27. J.K. Brosi and J.J. Lewandowski: *Scripta Mater.*, 2010, vol. 63, pp. 799–802.
28. C. Menzemer and T.S. Srivatsan: *Mater. Sci. Eng. A*, 1999, vol. A271, pp. 188–95.
29. K. Van Kranenburg, T. Riemslag, J. Zuidema, S. Benedictus-de Vries, and F. Veer: *Mater. Sci.*, 2001, vol. 37, pp. 970–74.
30. F. Ford: *Corrosion*, 1979, vol. 35, pp. 281–87.
31. J.K. Donald: *Fracture Mechanics Characterization of Aluminum Alloys for Marine Structural Applications, SSC-448*, Ship Structure Committee, Washington, DC, 2007.
32. P.S. Pao, R. Goswami, R.A. Bayles, T.M. Longazel, and R.L. Holtz: *Fatigue of Materials—Advances and Emergences of Understanding*, Eds. T.S. Srivatsan and M.A. Imam, Wiley, Hoboken, NJ, 2010, pp. 85–92.
33. J.S. Montgomery and E.S. Chin: *AMPTIAC Quart*, 2004, vol. 8 (4), pp. 15–20.
34. R.L. Holtz, P.S. Pao, R.A. Bayles, T.M. Longazel, and R. Goswami: *DoD Corrosion Conference Proceedings*, NACE International, Houston, TX, Paper 20421, 2011, in press.
35. R. Goswami, G. Spanos, P.S. Pao, and R.L. Holtz: *Metall. Mater. Trans. A*, 2011, vol. 42A, pp. 348–55.
36. R. Goswami, G. Spanos, P.S. Pao, and R.L. Holtz: *Mater. Sci. Eng. A*, 2010, vol. 527, pp. 1089–95.
37. ASTM E647-05, Standard Test Method for Measurement of Fatigue Crack Growth Rates, 2005.
38. D.O. Sprowls, M.B. Shumaker, J.D. Walsh, and J.W. Coursen: "Evaluation of Stress Corrosion Cracking Susceptibility using

Fracture Mechanics Techniques," Final Report, Contract Number NAS 8-21487, May 1973, Alcoa Laboratories, Pittsburgh, PA.

39. M. Liu, P. Schmutz, S. Zanna, A. Seyeux, H. Ardelean, G. Song, A. Atrens, and P. Marcus: *Corros. Sci.*, 2010, vol. 52, pp. 562–78.
40. Z. Xing, S. Yujui, and T. Mingjing: *Int. J. Fatigue*, 1991, vol. 13, pp. 69–72.
41. C.J. van der Wekken and M. Jassen: *J. Electrochem. Soc.*, 1991, vol. 138, pp. 2891–96.
42. S. Suresh: *Fatigue of Materials*, 1st ed., Cambridge University Press, New York, NY, 1991, pp. 245–47.
43. Z.M. Gasem and R.P. Gangloff: *Chemistry and Electrochemistry of Corrosion and Stress Corrosion Cracking: A Symposium Honoring the Contributions of R.W. Steahle*, Ed. R.H. Jones, TMS, Warrendale, PA, 2001, pp. 501–21.
44. J.S. Warner, S. Kim, and R.P. Gangloff: *Int. J. Fatigue*, 2009, vol. 31, pp. 1952–65.
45. R.H. Jones, V.Y. Gertsman, J.S. Vetrano, and C.F. Windisch: *Scripta Mater.*, 2004, vol. 50, pp. 1355–59.
46. ASTM E 1681-03, "Standard Test Method for Determining Threshold Stress Intensity Factor for Environment-Assisted Cracking of Metallic Materials," 2003.
47. F.S. Bovard: Alcoa Center, PA, Private communication, 2010.
48. S. Suresh: *Fatigue of Materials*, 1st ed., Cambridge University Press, New York, NY, 1991, pp. 380–82.
49. L. Hagn: *Mater. Sci. Eng. A*, 1988, vol. A103, pp. 193–205.
50. R.P. Wei: *Fatigue Fract. Eng. Mater. Struct.*, 2002, vol. 25, pp. 845–54.
51. I.P. Gnyp and V.I. Pokhmursky: *Mater. Sci.*, 1994, vol. 30, pp. 621–35.
52. R.P. Wei and G.W. Simmons: *Int. J. Fract.*, 1981, vol. 17, pp. 235–47.
53. K. Sadananda and A.K. Vasudevan: *Int. J. Fatigue*, 2004, vol. 26, pp. 39–47.
54. K. Sadananda, A.K. Vasudevan, and R.L. Holtz: *Int. J. Fatigue*, 2001, vol. 23, pp. S277–86.
55. K. Sadananda, A.K. Vasudevan, and I.W. Kang: *Acta Mater.*, 2003, vol. 51, pp. 3399–3414.
56. K. Sadananda and A.K. Vasudevan: *Int. J. Fatigue*, 2005, vol. 27, pp. 1255–66.
57. K. Sadananda and A.K. Vasudevan: *Fatigue Frac. Eng. Mater. Struct.*, 2003, vol. 26, pp. 835–45.
58. ASTM G-67-04, "Standard Test Method for Determining the Susceptibility to Intergranular Corrosion of 5XXX Series Aluminum Alloys by Mass Loss After Exposure to Nitric Acid (NAMLT Test)," 2004.